Nanoscale shift of the intensity distribution of dipole radiation

Jie Shu, Xin Li, and Henk F. Arnoldus*

Department of Physics and Astronomy, Mississippi State University, P.O. Drawer 5167, Mississippi State, Mississippi 39762-5167, USA
**Corresponding author: arnoldus@ra.msstate.edu*

Received October 9, 2008; revised December 3, 2008; accepted December 5, 2008; posted December 12, 2008 (Doc. ID 102571); published January 29, 2009

The energy flow lines (field lines of the Poynting vector) for radiation emitted by a dipole are in general curves, rather than straight lines. For a linear dipole the field lines are straight, but when the dipole moment of a source rotates, the field lines wind numerous times around an axis, which is perpendicular to the plane of rotation, before asymptotically approaching a straight line. We consider an elliptical dipole moment, representing the most general state of oscillation, and this includes the linear dipole as a special case. Due to the spiraling near the source, for the case of a rotating dipole moment, the field lines in the far field are displaced with respect to the outward radial direction, and this leads to a shift of the intensity distribution of the radiation in the far field. This shift is shown to be independent of the distance to the source and, although of nanoscale dimension, should be experimentally observable.

OCIS codes: 080.1235, 080.4865, 260.2110.

1. INTRODUCTION

In the short wavelength approximation (the geometrical optics limit), light appears to travel along straight lines from a source to an observer. These optical rays are the orthogonal trajectories of the wavefronts, and they coincide, in this approximation, with the field lines of the Poynting vector, representing the flow pattern of the electromagnetic energy [1]. We shall consider radiation emitted by a localized source near the origin of coordinates, and we shall assume a time-harmonic source, oscillating with angular frequency ω, so that the time-averaged Poynting vector $\mathbf{S}(\mathbf{r})$ is independent of time. The field lines of the Poynting vector for an exact solution of Maxwell's equations will in general be curves. In the far field, each curve approaches asymptotically a straight line, reminiscent of an optical ray. However, when a field line is curved close to the source, it may be expected that this has an effect on the field line distribution in the far field. Figure 1 shows a field line of the Poynting vector for the radiation emitted by a dipole, with a dipole moment that rotates counterclockwise in the xy plane. The scale in the figure is such that one wavelength corresponds to 2π. Near the dipole, the field line swirls around the z axis, and in the far field it approaches the straight line l. Due to the rotation near the source, the asymptotic line l is displaced with respect to the line m, which is parallel to l, but starts at the origin of coordinates. Therefore, it appears as if the radiation comes from a point in the xy plane, which does not coincide with the location of the source [2]. The spatial extend of the vortex in Fig. 1 is less than or about a wavelength, depending on the direction of observation and the state of oscillation of the dipole. The vortex structure of the field line of $\mathbf{S}(\mathbf{r})$ near the source has an effect in the far field, and it can be anticipated that the displacement shown for a single field line in Fig. 1 should lead to an observable shift of the intensity distribution of the radiation at a large distance.

2. POYNTING VECTOR FOR A DIPOLE

The dipole moment $\mathbf{d}(t)$ of an oscillating electric dipole can be written as

$$\mathbf{d}(t) = d_o \,\mathrm{Re}(\boldsymbol{\varepsilon} e^{-i\omega t}), \tag{1}$$

with d_o real and vector $\boldsymbol{\varepsilon}$ normalized as $\boldsymbol{\varepsilon}\cdot\boldsymbol{\varepsilon}^*=1$. The time-harmonic electric field is

$$\mathbf{E}(\mathbf{r},t) = \mathrm{Re}[\mathbf{E}(\mathbf{r})e^{-i\omega t}], \tag{2}$$

with $\mathbf{E}(\mathbf{r})$ being the complex amplitude; the magnetic field is represented similarly. For a dipole located at the origin of coordinates, the fields are [3]

$$\mathbf{E}(\mathbf{r}) = \frac{d_o k_o^3}{4\pi\varepsilon_o}\left\{\boldsymbol{\varepsilon} - (\boldsymbol{\varepsilon}\cdot\hat{\mathbf{r}})\hat{\mathbf{r}} + [\boldsymbol{\varepsilon} - 3(\boldsymbol{\varepsilon}\cdot\hat{\mathbf{r}})\hat{\mathbf{r}}]\frac{i}{q}\left(1+\frac{i}{q}\right)\right\}\frac{e^{iq}}{q}, \tag{3}$$

$$\mathbf{B}(\mathbf{r}) = -\frac{d_o k_o^3}{4\pi\varepsilon_o c}\boldsymbol{\varepsilon}\times\hat{\mathbf{r}}\left(1+\frac{i}{q}\right)\frac{e^{iq}}{q}, \tag{4}$$

with $k_o=\omega/c$, and we have set $q=k_o r$ for the dimensionless distance between the field point $\mathbf{r}$ and the location of the dipole. The Poynting vector

$$\mathbf{S}(\mathbf{r}) = \frac{1}{2\mu_o}\mathrm{Re}[\mathbf{E}(\mathbf{r})\times\mathbf{B}(\mathbf{r})^*], \tag{5}$$

can be evaluated, and the result is

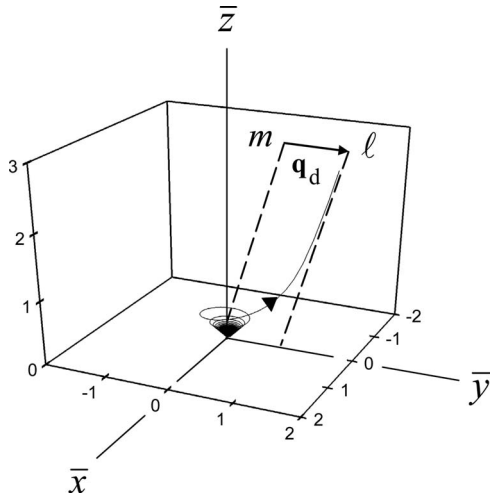

Fig. 1. Field line of the Poynting vector for a rotating dipole moment in the xy plane. At a large distance the field line approaches the line l. Line m is parallel to line l, but it starts at the origin of coordinates. The rotation of the field line near the source leads to an effective displacement of the field line in the far field, as compared to an optical ray that would emanate from the location of the dipole. We use dimensionless coordinates $\bar{x}=k_o x$, $\bar{y}=k_o y$, and $\bar{z}=k_o z$.

$$\mathbf{S}(\mathbf{r}) = \frac{3P_o}{8\pi r^2}\left\{[1-(\hat{\mathbf{r}}\cdot\boldsymbol{\varepsilon})(\hat{\mathbf{r}}\cdot\boldsymbol{\varepsilon}^*)]\hat{\mathbf{r}} - \frac{2}{q}\left(1+\frac{1}{q^2}\right)\mathrm{Im}[(\hat{\mathbf{r}}\cdot\boldsymbol{\varepsilon})\boldsymbol{\varepsilon}^*]\right\}, \tag{6}$$

with

$$P_o = \frac{ck_o^4 d_o^2}{12\pi\varepsilon_o}, \tag{7}$$

which equals the power emitted by the dipole. For a magnetic dipole, the electric and magnetic fields are different, but the resulting Poynting vector, Eq. (6), is the same.

Vector $\boldsymbol{\varepsilon}$ represents the state of oscillation of the dipole. When $\boldsymbol{\varepsilon}$ is real, we have $\mathbf{d}(t)=d_o\boldsymbol{\varepsilon}\cos(\omega t)$, and therefore the dipole moment oscillates back and forth along vector $\boldsymbol{\varepsilon}$ (linear dipole). The Poynting vector from Eq. (6) simplifies to

$$\mathbf{S}(\mathbf{r}) = \frac{3P_o}{8\pi r^2}[1-(\hat{\mathbf{r}}\cdot\boldsymbol{\varepsilon})^2]\hat{\mathbf{r}}. \tag{8}$$

At any field point $\mathbf{r}$ the Poynting vector is in the $\hat{\mathbf{r}}$ direction, and consequently the field lines of the vector field $\mathbf{S}(\mathbf{r})$ are straight lines in the radial direction. For an observation direction along the dipole axis, e.g., $\hat{\mathbf{r}}=\pm\boldsymbol{\varepsilon}$, we have $\mathbf{S}(\mathbf{r})=0$, which expresses the fact that no energy is emitted along the dipole axis. This makes the dipole axis a singular line of the field line pattern.

When we have $\boldsymbol{\varepsilon}=-(\mathbf{e}_x+i\mathbf{e}_y)/\sqrt{2}$, the dipole moment vector $\mathbf{d}(t)$ has a constant magnitude and rotates with angular frequency ω in the xy plane, and in the counterclockwise direction when viewed down the positive z axis. Such electric dipole radiation is emitted by an atom in a $\Delta m=-1$ electronic transition [4]. The rotation of the dipole moment gives a swirling of the field lines of $\mathbf{S}(\mathbf{r})$ around the z axis in the neighborhood of the dipole [5], as illustrated in Fig. 1. In Eq. (6), this rotation comes from the term with $\mathrm{Im}[(\hat{\mathbf{r}}\cdot\boldsymbol{\varepsilon})\boldsymbol{\varepsilon}^*]$. Since the term is proportional to $1/q$, it vanishes in the far field, and only the contribution proportional to $\hat{\mathbf{r}}$ in $\mathbf{S}(\mathbf{r})$ survives. Therefore, it may seem that since in the far field we have $\mathbf{S}(\mathbf{r})\propto\hat{\mathbf{r}}$, the field lines of $\mathbf{S}(\mathbf{r})$ should run in the radial direction. However, near the dipole a field line spirals around the z axis, so when it approaches a straight line in the far field, it is offset as compared to a field line that would emanate from the site of the dipole. This gives a displacement of the field lines in the far field, and hence a possible shift in the intensity distribution in the far field.

3. ANGULAR DISTRIBUTION OF THE EMITTED POWER

The power flowing through a surface element dA, located at point $\mathbf{r}$, into the direction of the unit normal $\hat{\mathbf{n}}$ on dA, is equal to $dP=\mathbf{S}(\mathbf{r})\cdot\hat{\mathbf{n}}dA$. We now consider dA as part of a sphere with radius r_o, and with the origin of coordinates as its center. Then the unit normal $\hat{\mathbf{n}}$ is equal to $\hat{\mathbf{r}}$ at any point, and we have $dA=r_o^2 d\Omega$, with $d\Omega$ the solid angle corresponding to the surface element dA. The emitted power per unit solid angle is then

$$\frac{dP}{d\Omega} = r_o^2\mathbf{S}(\mathbf{r})\cdot\hat{\mathbf{r}}, \tag{9}$$

and with Eq. (6) this yields

$$\frac{dP}{d\Omega} = \frac{3P_o}{8\pi}[1-(\hat{\mathbf{r}}\cdot\boldsymbol{\varepsilon})(\hat{\mathbf{r}}\cdot\boldsymbol{\varepsilon}^*)]. \tag{10}$$

Vector $\hat{\mathbf{r}}$ has the significance of the observation direction, and in terms of angles θ and ϕ of a spherical coordinate system this vector is

$$\hat{\mathbf{r}} = (\mathbf{e}_x\cos\phi + \mathbf{e}_y\sin\phi)\sin\theta + \mathbf{e}_z\cos\theta. \tag{11}$$

Therefore, $dP/d\Omega$ in Eq. (10) gives the radiation pattern as a function of θ and ϕ, given a particular value of vector $\boldsymbol{\varepsilon}$. When integrated over a 4π solid angle, the total emitted power is P_o.

The right-hand side of Eq. (10) is independent of the radius r_o of the sphere, and this may suggest that power simply flows radially outward, as for the case of a linear dipole, and as in the geometrical optics limit of light propagation. We see from Fig. 1 that the field lines of the Poynting vector wind around the z axis near the dipole, and the power flows out of the dipole along such field lines. The outward power flow $dP/d\Omega$ for a given observation direction (θ,ϕ) shows no sign of this rotation of the field lines in the near field for any r_o. The term with $\mathrm{Im}[(\hat{\mathbf{r}}\cdot\boldsymbol{\varepsilon})\boldsymbol{\varepsilon}^*]$ in Eq. (6) is responsible for the rotation of the field lines. With Eq. (9) we see that the contribution of this term becomes proportional to $\mathrm{Im}[(\hat{\mathbf{r}}\cdot\boldsymbol{\varepsilon})(\hat{\mathbf{r}}\cdot\boldsymbol{\varepsilon}^*)]$, and this is zero.

4. INTENSITY DISTRIBUTION OF THE RADIATION ON A PLANE

The angular distribution of the emitted power does not reveal the possible circulation of the field lines in the near field, no matter the radius r_o of the sphere. Figure 2

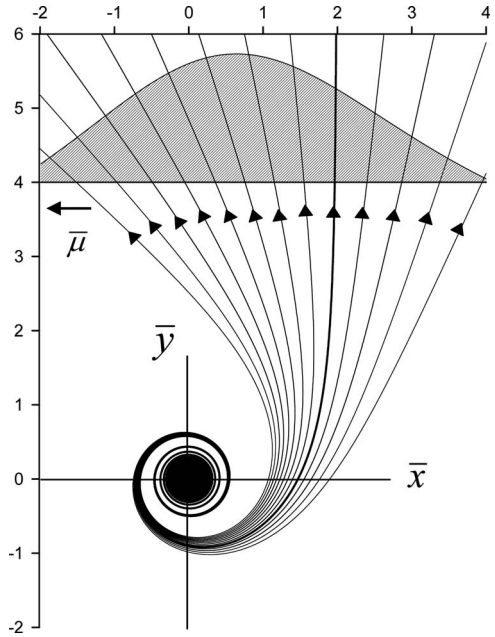

Fig. 2. Several field lines in the xy plane of the Poynting vector for the case of a counterclockwise rotating circular dipole in the xy plane. A bundle of field lines, as in the figure, determines the intensity distribution on an image plane (line $\bar{y}=4$). The bold field line is approximately perpendicular to the image plane, and runs asymptotically into the observation direction (θ_o, ϕ_o), which is $(\pi/2, \pi/2)$ in this illustration.

shows several field lines of the Poynting vector for a dipole rotating in the xy plane, and we clearly notice an asymmetry in the field line distribution, for instance along the line $\bar{y}=4$ (in dimensionless units, as in Fig. 1), which is due to the spiraling behavior of the field lines. To possibly observe the rotation of the field lines, we consider the intensity distribution of the radiation over an image plane, rather than over a sphere. We take the image plane as a tangent plane of a sphere with radius r_o, and the intersection point will be represented by vector $\mathbf{r}_o$. Therefore, the position of the plane is determined by angles (θ_o, ϕ_o), and by its perpendicular distance r_o to the origin. The unit vectors $\mathbf{e}_{\theta_o}$ and $\mathbf{e}_{\phi_o}$ lie in the image plane, as shown in Fig. 3, and they define a rectangular coordinate system (λ, μ) in which the coordinate axes are along the unit vectors. A point $\mathbf{r}$ in the image plane can then be represented as

$$\mathbf{r} = \mathbf{r}_o + \lambda \mathbf{e}_{\theta_o} + \mu \mathbf{e}_{\phi_o}. \tag{12}$$

The unit normal vector on the image plane is $\hat{\mathbf{r}}_o$ for every point in the plane. The intensity I (power per unit area) at point $\mathbf{r}$ in the plane depends on the location of the plane, specified by $\mathbf{r}_o$, and on the coordinates (λ, μ) of the point with respect to the origin of the plane at $\mathbf{r}_o$. The intensity distribution over the plane is therefore

$$I(\mathbf{r}_o; \lambda, \mu) = \mathbf{S}(\mathbf{r}) \cdot \hat{\mathbf{r}}_o, \tag{13}$$

with $\mathbf{S}(\mathbf{r})$ given by Eq. (6). We introduce dimensionless coordinates $\bar{\lambda}=k_o\lambda$, $\bar{\mu}=k_o\mu$ in the image plane. Since k_o is the wavenumber, a dimensionless distance of 2π represents one wavelength. Similarly, $q_o=k_o r_o$ is the dimensionless distance between the dipole and the image plane,

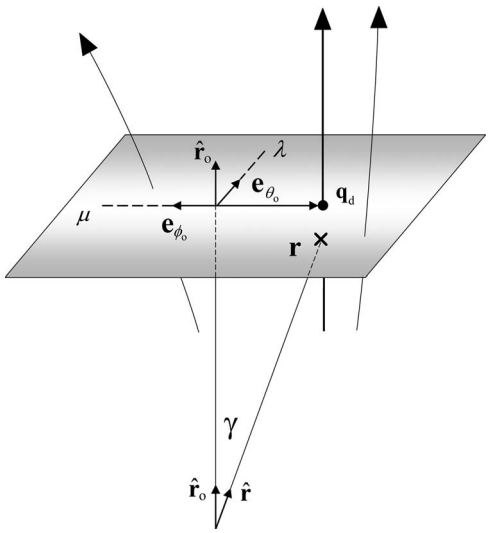

Fig. 3. Image plane is spanned by the unit vectors $\mathbf{e}_{\theta_o}$ and $\mathbf{e}_{\phi_o}$, and λ and μ are the corresponding Cartesian coordinates in the plane. Field lines of the Poynting vector that cross this plane determine the intensity profile, formed on the plane. The bold field line runs asymptotically in the $\hat{\mathbf{r}}_o$ direction, and crosses the plane at the location given by the displacement vector $\mathbf{q}_d$ with respect to the origin of the plane. This is the same $\mathbf{q}_d$ as in Fig. 1. Angle γ is the angle between the observation direction (θ_o, ϕ_o), represented by $\hat{\mathbf{r}}_o$, and the angular location of the field point $\mathbf{r}$ in the observation plane, as seen from the site of the source.

and for point $\mathbf{r}$ in the plane we have

$$q = \sqrt{q_o^2 + \bar{\lambda}^2 + \bar{\mu}^2}, \tag{14}$$

as the dimensionless distance between this point and the position of the dipole. From Eq. (12) we obtain

$$\hat{\mathbf{r}} = \frac{1}{q}(q_o \hat{\mathbf{r}}_o + \bar{\lambda}\mathbf{e}_{\theta_o} + \bar{\mu}\mathbf{e}_{\phi_o}), \tag{15}$$

and therefore we have $\hat{\mathbf{r}} \cdot \hat{\mathbf{r}}_o = q_o/q$. The intensity distribution then becomes

$$I(\mathbf{r}_o; \lambda, \mu) = I_o \left(\frac{q_o}{q}\right)^3 \left\{ 1 - (\hat{\mathbf{r}} \cdot \boldsymbol{\varepsilon})(\hat{\mathbf{r}} \cdot \boldsymbol{\varepsilon}^*) - \frac{2}{q_o}\left(1 + \frac{1}{q^2}\right) \times \mathrm{Im}[(\hat{\mathbf{r}} \cdot \boldsymbol{\varepsilon})(\hat{\mathbf{r}}_o \cdot \boldsymbol{\varepsilon}^*)] \right\}, \tag{16}$$

with

$$I_o = \frac{3P_o}{8\pi r_o^2}. \tag{17}$$

In Eq. (16), $\hat{\mathbf{r}}$ is given by Eq. (15) and $\hat{\mathbf{r}}_o$ follows from Eq. (11) with (θ, ϕ) replaced by (θ_o, ϕ_o).

The contribution $1-(\hat{\mathbf{r}}\cdot\boldsymbol{\varepsilon})(\hat{\mathbf{r}}\cdot\boldsymbol{\varepsilon}^*)$ in Eq. (16) is essentially $\mathrm{d}P/\mathrm{d}\Omega$, as can be seen from Eq. (10), and this part corresponds to the energy flow in the radial direction. The term in braces containing $\mathrm{Im}[(\hat{\mathbf{r}}\cdot\boldsymbol{\varepsilon})(\hat{\mathbf{r}}_o\cdot\boldsymbol{\varepsilon}^*)]$ arises due to the rotation of the field lines. The overall factor $(q_o/q)^3$ has two contributions: A factor $(q_o/q)^2$ comes from $\mathbf{S}(\mathbf{r})$, Eq. (6), being proportional to $1/r^2$, and a factor q_o/q results from $\hat{\mathbf{r}}\cdot\hat{\mathbf{r}}_o = q_o/q$, e.g., from projecting the radial outflow onto a plane rather than a sphere. In other words, the factor

q_o/q accounts for the fact that the field lines are not perpendicular to the observation plane, as can be seen in Fig. 2.

An intensity distribution $I_o(q_o/q)^3$ in the image plane would be a single peak at the origin, and rotational symmetric around the normal vector $\hat{\mathbf{r}}_o$. If we set $q_o/q=\cos\gamma$, then γ (see Fig. 3) is the angle between vectors $\mathbf{r}$ and $\mathbf{r}_o$, as seen from the location of the dipole. The angular half-width at half-maximum of the image on the plane, as viewed from the site of the dipole, then follows from $(q_o/q)^3=1/2$, and this is $\gamma=37°$. This peak will be altered due to the angular dependence of the emitted power in the radial direction and due to possible rotations of the field lines.

As an example, let us consider a linear dipole along the y axis, so $\boldsymbol{\varepsilon}=\mathbf{e}_y$. Since $\boldsymbol{\varepsilon}$ is real, the field lines of the Poynting vector are in the radial direction, without any curving. We take the image plane perpendicular to the y axis, and therefore $\boldsymbol{\varepsilon}$ coincides with the observation direction $\hat{\mathbf{r}}_o$. Equation (16) can then be simplified to

$$I(\mathbf{r}_o;\lambda,\mu)=I_o\cos^3\gamma\sin^2\gamma, \tag{18}$$

where γ is the angular location of a point on the image plane, as illustrated in Fig. 3. The intensity in the observation direction ($\gamma=0$) is zero, and therefore the intensity has a minimum at the origin of the image plane. The intensity is rotational symmetric around $\hat{\mathbf{r}}_o$, and consequently the maximum of the distribution has the shape of a ring. Figure 4 shows the intensity distribution for this case. The angular width of the ring is given by $\cos\gamma=\sqrt{3/5}$, which gives $\gamma=39°$, and the radius of the ring in the image plane is $q_o\sqrt{2/3}$.

5. ELLIPTICAL DIPOLE MOMENT

Features of the intensity distribution like the ring in Fig. 4 are of macroscopic nature in the sense that they scale with the distance q_o between the dipole and the image plane. The structure of the intensity profile is a result of the angular distribution of the emitted power, $dP/d\Omega$. On the other hand, the swirling of the field lines, as in Fig. 2, can only affect the intensity on a nanoscale, since the spatial dimension of the vortex is of the order of a wavelength of the radiation. We shall now consider the effect of the rotation of the field lines on the intensity distribution in detail.

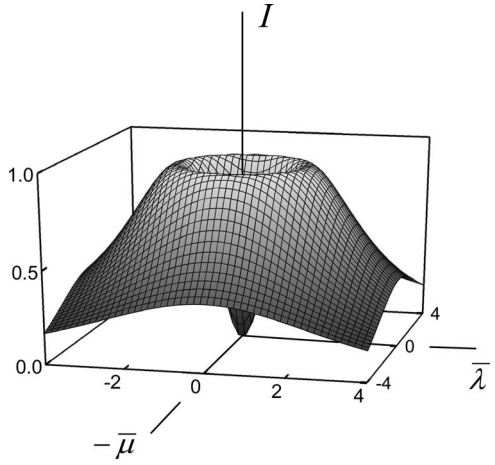

Fig. 4. Graph of the intensity distribution in an image plane perpendicular to the y axis, for a dipole moment which oscillates linearly along the y axis. The dimensionless distance between the plane and the dipole is $q_o=2$, and the dimensionless radius of the ring is 1.63.

For an arbitrary complex-valued vector $\boldsymbol{\varepsilon}$, the dipole moment $\mathbf{d}(t)$ in Eq. (1) traces out an ellipse in a plane [6,7]. We take this plane as the xy plane and parametrize vector $\boldsymbol{\varepsilon}$ as

$$\boldsymbol{\varepsilon}=-\frac{1}{\sqrt{\beta^2+1}}(\beta\mathbf{e}_x+i\mathbf{e}_y),\quad \beta \text{ real}. \tag{19}$$

For $\beta>0$ ($\beta<0$) the dipole moment rotates in the counterclockwise (clockwise) direction, when viewed down the z axis, and for $\beta=\pm1$ the ellipse reduces to a circle. For $\beta=0$ the oscillation becomes linear along the y axis. The unit vector $\hat{\mathbf{r}}$ into the direction of a point on the image plane involves the unit vectors that span the plane, according to Eq. (15). Explicitly we have

$$\mathbf{e}_{\theta_o}=(\mathbf{e}_x\cos\phi_o+\mathbf{e}_y\sin\phi_o)\cos\theta_o-\mathbf{e}_z\sin\theta_o, \tag{20}$$

$$\mathbf{e}_{\phi_o}=-\mathbf{e}_x\sin\phi_o+\mathbf{e}_y\cos\phi_o, \tag{21}$$

and the intensity becomes

$$I(\mathbf{r}_o;\lambda,\mu)=I_o\left(\frac{q_o}{q}\right)^3\left[1-(\hat{\mathbf{r}}\cdot\boldsymbol{\varepsilon})(\hat{\mathbf{r}}\cdot\boldsymbol{\varepsilon}^*)-\frac{1}{q_oq}\left(1+\frac{1}{q^2}\right)\frac{2\beta}{\beta^2+1}\bar{\mu}\sin\theta_o\right]. \tag{22}$$

The last term in square brackets comes from the rotation of the field lines. We notice that this term is proportional to the coordinate $\bar{\mu}$ in the image plane, and this indicates that the peak in the intensity distribution will be shifted along the $\bar{\mu}$ axis. We also see that for $\beta>0$, as in Fig. 2, the shift is in the negative $\bar{\mu}$ direction, and for $\beta<0$ the shift is in the positive direction. For a linear dipole ($\beta=0$), the shift vanishes, and for an observation direction $\hat{\mathbf{r}}_o$ perpendicular to the plane of rotation of the dipole ($\theta_o=0$ or π), the shift is zero for any β. The displacement term has an overall factor of $1/(q_oq)$, which is $\mathcal{O}(1/q_o^2)$ in the far field ($q_o\to\infty$), and it may seem that at a large distance from the source, the shift of the peak should disappear. We shall see in Section 6 that this is not the case.

The first part in square brackets in the expression (22) for $I(\mathbf{r}_o;\lambda,\mu)$ comes from $dP/d\Omega$, and for an elliptic dipole we find explicitly:

$$(\hat{\mathbf{r}}\cdot\boldsymbol{\varepsilon})(\hat{\mathbf{r}}\cdot\boldsymbol{\varepsilon}^*)=\frac{1}{q^2}\frac{1}{\beta^2+1}[\beta^2(\bar{\rho}\cos\phi_o-\bar{\mu}\sin\phi_o)^2+(\bar{\rho}\sin\phi_o+\bar{\mu}\cos\phi_o)^2]. \tag{23}$$

Here we have introduced the abbreviation

$$\bar{\rho}=q_o\sin\theta_o+\bar{\lambda}\cos\theta_o. \tag{24}$$

6. EXTREMUM IN THE INTENSITY PROFILE IN THE FAR FIELD FOR A CIRCULAR DIPOLE

When the dipole moment rotates in a circle, we have $\beta = \pm 1$, and the expression for the intensity distribution on a plane simplifies considerably. From Eqs. (22) and (23) we obtain

$$I(\mathbf{r}_o;\bar{\lambda},\bar{\mu}) = I_o\left(\frac{q_o}{q}\right)^3\left[1-\frac{1}{2q^2}(\bar{\rho}^2+\bar{\mu}^2) - \frac{\beta}{q_o q}\left(1+\frac{1}{q^2}\right)\bar{\mu}\sin\theta_o\right]. \quad (25)$$

The dependence on the observation direction ϕ_o has disappeared, as could be expected for a circular dipole. The last term in square brackets comes from the curving of the field lines near the dipole, as in Figs. 1 and 2, and this term is proportional to $\bar{\mu}$. The displacement $\mathbf{q}_d$ of the field lines in the far field is in the $\bar{\mu}$ direction, and we expect a corresponding shift of the intensity distribution in the image plane. When considering the $\bar{\mu}$ dependence of $I(\mathbf{r}_o;\bar{\lambda},\bar{\mu})$ for fixed $\bar{\lambda}$, the dependence on $\bar{\mu}$ enters through the parameter q, Eq. (14), and explicitly as $\bar{\mu}^2$ and $\bar{\mu}$ in Eq. (25). Without the rotation of the field lines, $\bar{\mu}$ only enters as $\bar{\mu}^2$ and since this is symmetric in $\bar{\mu}$ the profile would be symmetric in the $\bar{\mu}$ direction around $\bar{\mu}=0$ in the image plane. In particular, the point $\bar{\mu}=0$ would be either a local maximum or minimum, and hence any shift of this local extremum would be a reflection of the circulation of the field lines in the optical near field.

To find the extrema of the intensity distribution, we first consider the dependence of $I(\mathbf{r}_o;\bar{\lambda},\bar{\mu})$ on $\bar{\mu}$, for a given $\bar{\lambda}$. Setting $\partial I/\partial\bar{\mu}=0$ yields

$$\bar{\mu}\left[4-\frac{5}{2q^2}(\bar{\mu}^2+\bar{\rho}^2)\right] = -\beta\frac{\sin\theta_o}{q_o q}(q_o^2+\bar{\lambda}^2-3\bar{\mu}^2), \quad (26)$$

and here we have also assumed detection in the far field, for which $q_o \gg 1$. For detection along the z axis ($\theta_o=0$ or π) we have $\sin\theta_o=0$, and a solution is $\bar{\mu}=0$. To find the general solution, we recall that an extremum in the far field should scale with q_o, so that angle γ in Fig. 3 remains constant. When we divide Eq. (26) by q_o, then the left-hand side becomes constant for q_o large, and the right-hand side vanishes as $\mathcal{O}(1/q_o)$. It can be shown by inspection that the factor in square brackets on the left-hand side is positive, and therefore we find from Eq. (26) that $\bar{\mu}/q_o=0$ for any given $\bar{\lambda}$. Since there is only one solution, the extremum is a maximum in the $\bar{\mu}$ direction. Similarly, $\partial I/\partial\bar{\lambda}=0$ yields

$$-3\bar{\lambda}+\frac{5\bar{\lambda}}{2q^2}(\bar{\mu}^2+\bar{\rho}^2)-\bar{\rho}\cos\theta_o = -\beta\frac{4\bar{\lambda}\bar{\mu}}{q_o q}\sin\theta_o, \quad (27)$$

for $q_o \gg 1$. For detection along the z axis ($\theta_o=0$ or π) we have $\bar{\rho}=\bar{\lambda}\cos\theta_o$, and we see that $\bar{\lambda}=0$ is a solution of Eq. (27). Also for detection in the xy plane, for which $\theta_o=\pi/2$, we find that $\bar{\lambda}=0$ is a solution. When we divide Eq. (27) by q_o, then the right-hand side goes to zero, and the remaining equation can be solved for $\bar{\lambda}/q_o$ for any given $\bar{\mu}/q_o$ and θ_o. The equation has one solution, and therefore the extremum in the $\bar{\lambda}$ direction is a maximum.

It follows from the previous paragraph that the intensity distribution has a single peak in the $\bar{\lambda}\bar{\mu}$ plane. When we indicate the coordinates of the location of the peak by $(\bar{\lambda}_p,\bar{\mu}_p)$, then we have $\bar{\mu}_p/q_o=0$. With $\bar{\mu}_p/q_o=0$, Eq. (27) becomes an equation for $\bar{\lambda}_p/q_o$, after division by q_o. When we set $\alpha=\bar{\lambda}_p/q_o$, Eq. (27) yields

$$\frac{5}{2}\alpha(\sin\theta_o+\alpha\cos\theta_o)^2 = (1+\alpha^2)[\sin\theta_o\cos\theta_o+\alpha(3+\cos^2\theta_o)], \quad (28)$$

which is a cubic equation for α, given the observation angle θ_o. The solution of this equation is shown in Fig. 5. We see that α is relatively small for all θ_o, so that a reasonable approximation is obtained by setting $\alpha^3\approx 0$, $\alpha^2\approx 0$. This yields

$$\alpha \approx \frac{\sin(2\theta_o)}{7\sin^2\theta_o - 8}, \quad (29)$$

which is shown as the dashed curve in the figure. The shift of the maximum in the $\bar{\lambda}$ direction is negative (positive) for $0<\theta_o<\pi/2$ ($\pi/2<\theta_o<\pi$).

7. SHIFT OF THE PEAK IN THE FAR FIELD FOR A CIRCULAR DIPOLE

The peak in the intensity distribution is located at $\bar{\lambda}_p = \alpha q_o$ along the $\bar{\lambda}$ axis in the image plane, where α follows from Fig. 5, given angle θ_o. The location of the peak is a consequence of the angle dependence of $dP/d\Omega$, and is independent of the rotation of the field lines near the origin of coordinates. The position scales with the distance q_o between the image plane and the dipole, such that the viewing angle γ is independent of q_o. In the $\bar{\mu}$ direction, the maximum appears at $\bar{\mu}_p/q_o=0$, and this leaves the possibility that $\bar{\mu}_p$ is finite, rather than zero. When we set $\bar{\mu}_p/q_o=0$ and $\bar{\lambda}_p/q_o=\alpha$ in Eq. (26), we obtain an equation for $\bar{\mu}_p$. The solution is

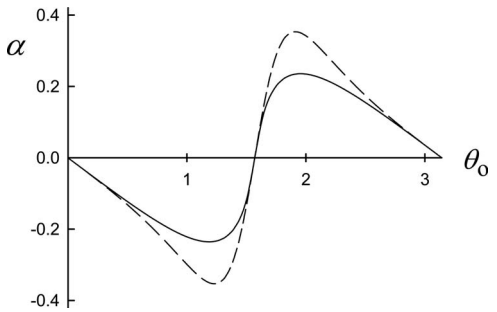

Fig. 5. Solid curve shows α, the solution of Eq. (28), as a function of θ_o, and the dashed curve is the approximation given by Eq. (29).

$$\bar{\mu}_p = -\beta(1+\alpha^2)^{3/2}\frac{2\sin\theta_o}{8(1+\alpha^2)-5(\sin\theta_o+\alpha\cos\theta_o)^2}, \quad (30)$$

which is independent of q_o, and represents the shift of the maximum in the far field. For a given θ_o, α follows from Eq. (28), and hence the shift of the peak along the $\bar{\mu}$ axis is a function of the observation angle θ_o only (apart from the overall $\beta=\pm1$). Figure 6 shows the far-field intensity distribution for $\theta_o=\pi/2$ with $\beta=1$. The maximum along the $\bar{\mu}$-axis is located at $\bar{\mu}_p=-2/3$.

The shift of the peak, $\bar{\mu}_p$, is zero for $\theta_o=0$, π and maximum for $\theta_o=\pi/2$, and the maximum shift at $\theta_o=\pi/2$ is $|\bar{\mu}_p|=2/3$. Figure 7 shows the behavior of the shift as a function of θ_o for $\beta=1$. The shift is due to the rotation in the field lines of the Poynting vector, and we see from Fig. 2 that the shift is expected to be negative for a dipole moment which rotates counterclockwise in the xy-plane. The right-hand side of Eq. (30) changes sign with β, and therefore for a clockwise rotating dipole moment the shift is positive. When the dipole radiation is emitted by an atom in a laser beam, the rotation direction of the dipole moment can be reversed by changing the helicity of the driving laser from left-circular to right-circular polarized, or vice versa, for instance by inserting a half-wave-plate. The peak in the intensity would then shift over 4/3 in dimensionless units, and this corresponds to a distance of $2\lambda/(3\pi)$, with λ being the wavelength of the radiation. Although this shift is of nanoscale size, it should be observable in experiment. In this fashion, the swirling of the field lines of the Poynting vector in the near field could be observed by a measurement in the far field.

All field lines of the Poynting vector run radially outward in the far field, but they are displaced with respect to an optical ray that would emanate from the exact site of the dipole, as illustrated in Fig. 1. For a given observation direction (θ_o,ϕ_o), there is one field line that runs exactly into that direction, and this field line intersects the observation plane under a right angle (bold field line in Fig. 2). The displacement vector of this field line is a vector in the corresponding observation plane, and this vector is along the $\bar{\mu}$ axis. If we write $\mathbf{q}_d=\bar{\mu}_d\mathbf{e}_{\phi_o}$, then the displacement of this field line is given by [8]

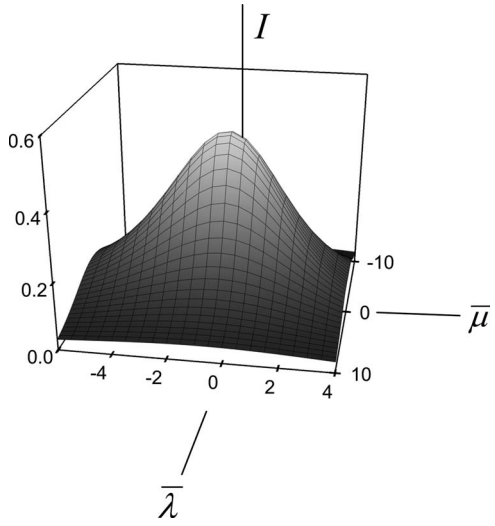

Fig. 6. Graph shows the far-field intensity distribution for a rotating dipole with $\beta=1$ for observation along the xy plane. The maximum is located on the $\bar{\mu}$ axis at $\bar{\mu}_p=-2/3$.

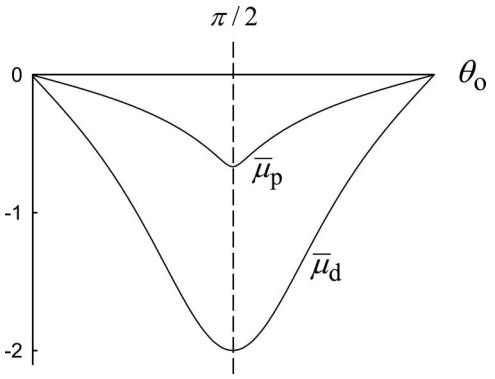

Fig. 7. Shift $\bar{\mu}_p$ of the peak in the intensity distribution and the displacement $\bar{\mu}_d$ of the central field line as a function of the observation angle θ_o, both for a circular dipole with $\beta=1$. For $\beta=-1$ both functions change sign.

$$\bar{\mu}_d = -\beta\frac{2\sin\theta_o}{2-\sin^2\theta_o}. \quad (31)$$

Both $\bar{\mu}_p$ and $\bar{\mu}_d$ are shown in Fig. 7, and we see that the displacement of the field line is larger than the shift of the peak in the corresponding intensity distribution. The intensity profile is determined by a bundle of field lines, as depicted in Fig. 2, and the direction of the central field line does not necessarily coincide exactly with the location of an extremum in the intensity pattern.

8. FAR FIELD INTENSITY PATTERN FOR AN ELLIPTICAL DIPOLE

In the most general state of oscillation of a dipole, the dipole moment vector traces out an ellipse, and the plane of this ellipse is taken as the xy plane. The ellipticity is represented by parameter β in Eq. (19). For $\beta=0$ the dipole moment oscillates linearly along the y axis. For $\beta=\pm1$ it rotates along a circle, and for $\beta\to\pm\infty$ the oscillation becomes linear along the x axis. We shall consider an observation plane perpendicular to the y axis, so that $\theta_o=\phi_o=\pi/2$. For this example, the intensity becomes

$$I(\mathbf{r}_o;\lambda,\mu) = I_o\left(\frac{q_o}{q}\right)^3\left\{1-\frac{1}{q^2(\beta^2+1)}\left[\beta^2\bar{\mu}^2+q_o^2 + 2\beta\bar{\mu}\frac{q}{q_o}\left(1+\frac{1}{q^2}\right)\right]\right\}. \quad (32)$$

For $\beta=0$ the profile has a minimum at $\bar{\lambda}=\bar{\mu}=0$ and a ring-shaped maximum, as shown in Fig. 4. For $\beta=0$ we have a linear dipole, and the field lines of the Poynting vector run in the radial direction, without any curving. Therefore, there is no shift $\bar{\mu}_p$ of the extremum (the hole in this case) in the far field. For $\beta=\pm1$, the extremum is a peak at $\bar{\lambda}=0$ and near $\bar{\mu}=0$, as shown in Fig. 6 for $\beta=1$. The shift of the peak in the $\bar{\mu}$ direction is $\bar{\mu}_p=-2\beta/3$.

Possible extrema along the $\bar{\lambda}$ axis follow from setting $\partial I/\partial\bar{\lambda}=0$, $\bar{\mu}=0$, and we also let $q_o\gg1$ for the far field. This yields $\bar{\lambda}=0$ and

$$\frac{\bar{\lambda}}{q_o} = \pm \sqrt{\frac{2-3\beta^2}{3(\beta^2+1)}}, \quad |\beta| < \sqrt{2/3}. \tag{33}$$

When $|\beta| < \sqrt{2/3}$, we obtain two solutions $\bar{\lambda}/q_o$, in addition to the solution $\bar{\lambda}=0$. This corresponds to two maxima and a minimum at $\bar{\lambda}=0$. When $|\beta| > \sqrt{2/3}$, we only have $\bar{\lambda}=0$, and therefore this must be a maximum. Similarly, extrema along the $\bar{\mu}$ axis follow from setting $\partial I/\partial\bar{\mu}=0$ and $\bar{\lambda}=0$. This gives

$$\bar{\mu}\left[5\beta^2+3-\frac{5}{q^2}(q_o^2+\beta^2\bar{\mu}^2)\right] = -\frac{2\beta}{q_o q}(q_o^2-3\bar{\mu}^2). \tag{34}$$

When dividing by q_o, the right-hand side vanishes in the far field. We then obtain the solutions $\bar{\mu}/q_o=0$ and

$$\frac{\bar{\mu}}{q_o} = \pm \sqrt{\frac{2-5\beta^2}{3}}, \quad |\beta| < \sqrt{2/5}. \tag{35}$$

We also find either two maxima and a minimum or one maximum, depending on the value of $|\beta|$.

For $\beta=0$ we have a minimum in both the $\bar{\lambda}$ and $\bar{\mu}$ directions at the origin of the image plane, as shown in Fig. 4, and the maximum has the shape of a ring. When $|\beta|$ increases, the locations of the maxima along the coordinate axes change according to Eqs. (33) and (35). These functions of $|\beta|$ are shown in Fig. 8, and we see that the dimension of the hole decreases both along the $\bar{\lambda}$ and $\bar{\mu}$ axes. Since the decrease along the $\bar{\mu}$ axis is faster than along the $\bar{\lambda}$ axis, the ring distorts. The dimension of the hole shrinks in both directions, and the hole becomes shallower. When $|\beta|$ approaches the value of $\sqrt{2/5}$, the maxima along the $\bar{\mu}$ axis approach the origin of coordinates, and for $|\beta| > \sqrt{2/5}$ we only have a maximum at $\bar{\mu}/q_o=0$. When $|\beta|$ increases further towards $|\beta|=\sqrt{2/3}$, also the maxima along the $\bar{\lambda}$ axis approach the origin, and for $|\beta| > \sqrt{2/3}$ we have a maximum at $\bar{\lambda}=0$. Therefore, for $0 \leqslant |\beta| < \sqrt{2/5}$ the intensity profile has a hole near the origin. For $\sqrt{2/5} < |\beta| < \sqrt{2/3}$ the region around the origin has the appearance of a saddle point, and for $|\beta| > \sqrt{2/3}$ we have a single peak, as for $\beta=1$ in Fig. 6.

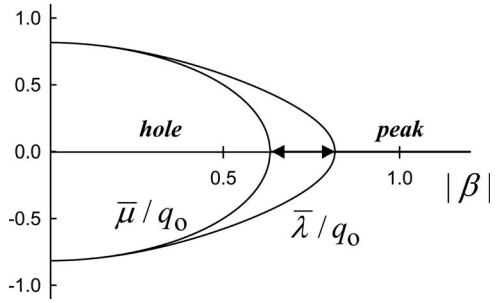

Fig. 8. Location of the maxima along the coordinate axes in the $\bar{\lambda}\bar{\mu}$ plane as a function of $|\beta|$. For $|\beta| < \sqrt{2/5}$ there are two maxima along both axes, and there is a hole in the middle. For $|\beta| > \sqrt{2/3}$ there is a single peak near the origin of coordinates. In the region indicated by the double-headed arrow there is a minimum along the $\bar{\lambda}$ direction and a maximum along the $\bar{\mu}$ direction near the origin.

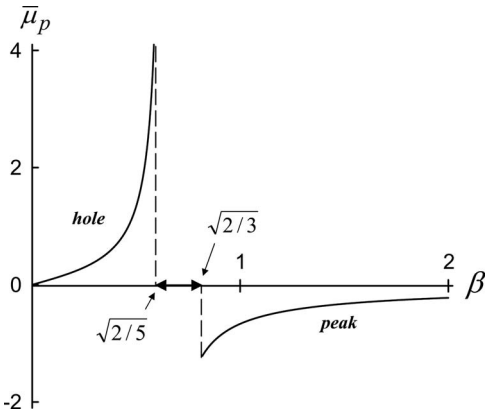

Fig. 9. The shift $\bar{\mu}_p$ for $\beta \geqslant 0$ of either the hole or the peak with respect to the origin of coordinates. In the transition region $\sqrt{2/5} < \beta < \sqrt{2/3}$, there is neither a hole nor a peak in the intensity distribution.

At the center of the profile we have minimum, a maximum, or a transition between the two, and at the location of this extremum we have $\bar{\lambda}=0$ and $\bar{\mu}/q_o=0$. Just as for the circular dipole, the condition $\bar{\mu}/q_o=0$ leaves open the possibility that $\bar{\mu}$ is finite. In Eq. (34) we let $\bar{\mu}/q_o \to 0$. We then obtain for the coordinates of the extremum around the origin of the image plane

$$\bar{\lambda}_p = 0, \quad \bar{\mu}_p = \frac{2\beta}{2-5\beta^2}. \tag{36}$$

The finite shift $\bar{\mu}_p$ is again a result of the rotation in the field lines near the source. Figure 9 shows $\bar{\mu}_p$ as a function of β for β positive. For $0 \leqslant \beta < \sqrt{2/5}$ the extremum is a hole, and Eq. (36) represents the shift of the hole with respect to the origin. We see from the figure that the shift of the hole is in the positive $\bar{\mu}$ direction. In the region $\beta > \sqrt{2/3}$, the extremum is a peak, and the shift is in the negative direction. For β negative, the hole shifts in the negative direction and the peak shifts in the positive direction. For a circular dipole we have $|\beta|=1$ and the magnitude of the shift of the peak is equal to $|\bar{\mu}_p|=2/3$, as in Fig. 6. This shift increases with decreasing $|\beta|$, and at $|\beta|=\sqrt{2/3}$ the magnitude of the shift is $|\bar{\mu}_p|=\sqrt{3/2}$. This is a factor of 1.84 larger than the shift for a circular dipole. The shift of the hole for $|\beta| < \sqrt{2/5}$ can be extremely large, but the depth and sharpness of the hole decrease with increasing shift.

9. INTENSITY IN THE NEAR FIELD

Thus far we have considered the intensity distribution in the far field. With contemporary experimental techniques [9,10] it has become feasible to detect electromagnetic radiation with nanoscale resolution very close to a source. In these experiments the electric field vector is measured, including its direction, within a fraction of a wavelength from the source. From these measurements, a field line pattern for the electric field can be obtained, and it should be possible to construct the field lines of the Poynting vector from these data. Figure 10 shows a typical intensity distribution on an image plane in the near field for a rotating dipole moment. The positive peak at the left-hand

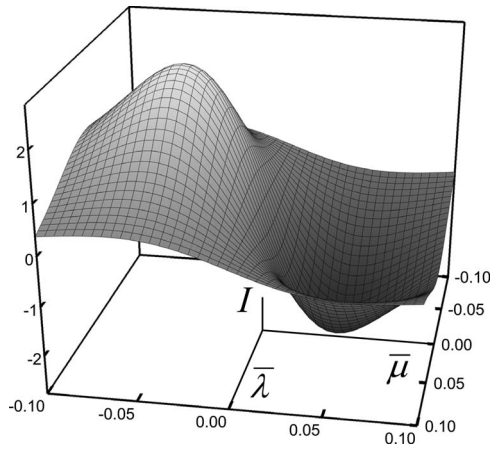

Fig. 10. Near-field intensity distribution for a dipole with $\beta=1$, observed in an image plane perpendicular to the y axis ($\theta_o=\phi_o=\pi/2$), shows a positive and a negative extremum. This is due to the fact that the field lines of the Poynting vector cross the plane in the outward direction at the negative $\bar{\mu}$ side, and re-enter the image plane at the positive $\bar{\mu}$ side. This profile is a result of the numerous rotations of the field lines around the z axis close to the source, as shown in Fig. 2.

side comes from the field lines passing through the plane in the outward direction, and the negative peak on the right represents field lines passing the plane in the opposite direction. This image is a direct consequence of the spiraling of the field lines near the source. A field line can pass through the plane on the left, and then this same field line can cross the image plane again in the opposite direction on the right.

10. CONCLUSIONS

The field lines of the Poynting vector for dipole radiation swirl around an axis in the near field, and approach a straight line in the far field, except for a linear dipole for which the field lines are straight at all distances to the source. This vortex structure, shown in Fig. 1, has the dimension of an optical wavelength or less, so it manifests itself in the near field. However, as also shown in Fig. 1, it leads to an asymptotic displacement of the field lines in the far field. To observe indirectly the existence of the vortex in the near field, we consider the intensity distribution in the far field, and as suggested in Fig. 2, we anticipate that the displacement of the field lines due to the vortex in the near field will yield a shift of the intensity profile in the far field.

We have considered the intensity distribution on a plane in the far field for a dipole with an elliptical dipole moment, rotating in the xy plane. In the image plane we define a rectangular coordinate system (λ,μ), associated with the spherical-coordinate angles (θ_o,ϕ_o) of the location of the image plane, as illustrated in Fig. 3. For a circular dipole, the intensity distribution is a single peak in the image plane. The maximum along the λ axis is located at $\bar{\lambda}_p=\alpha q_o$ (in dimensionless coordinates), where α is a function of the angle θ_o of the image plane, as shown in Fig. 5. The location of this maximum scales with q_o, which is the dimensionless distance between the dipole and the image plane. Therefore, the position of this maximum along the λ axis is simply a result of the non-uniformity of the emitted power per unit solid angle. The position of the maximum along the μ axis is given by Eq. (30), and this position does not scale with q_o. It is a finite shift of the peak, resulting from the displacement of the field lines of the Poynting vector, and it is due to the presence of the vortex in the near field. In this fashion, a near field phenomenon is reflected in a far field intensity profile, and therefore it should be possible to verify the existence of the vortex through a far field measurement.

REFERENCES

1. M. Born and E. Wolf, *Principles of Optics*, 6th ed. (Pergamon, 1980), Chap. 3.
2. H. F. Arnoldus, X. Li, and J. Shu, "Subwavelength displacement of the far-field image of a radiating dipole," Opt. Lett. **33**, 1446–1448 (2008).
3. J. D. Jackson, *Classical Electrodynamics*, 3rd ed. (Wiley, 1991), p. 411.
4. C. T. Cohen-Tannoudji, B. Diu, and F. Laloë, *Quantum Mechanics* (Wiley, 1977), Vol. 1, p. 838.
5. H. F. Arnoldus and J. T. Foley, "The dipole vortex," Opt. Commun. **231**, 115–128 (2004).
6. I. V. Lindell, *Methods for Electromagnetic Field Analysis* (Oxford U. Press, 1992), Sec. 1.4.
7. L. Mandel and E. Wolf, *Optical Coherence and Quantum Optics* (Cambridge U. Press, 1995), p. 469.
8. J. Shu, X. Li, and H. F. Arnoldus, "Energy flow lines for the radiation emitted by a dipole," J. Mod. Opt. **55**, 2457–2471 (2008).
9. K. G. Lee, H. W. Kihm, J. E. Kihm, W. J. Choi, H. Kim, C. Ropers, D. J. Park, Y. C. Yoon, S. B. Choi, D. H. Woo, J. Kim, B. Lee, Q. H. Park, C. Lienau, and D. S. Kim, "Vector field microscopic imaging of light," Nat. Photonics **1**, 53–56 (2007).
10. Y. Ohdaira, T. Inoue, H. Hori, and K. Kitahara, "Local circular polarization observed in surface vortices of optical near-fields," Opt. Express **16**, 2915–2921 (2008).